

THERMAL FLAVOR PRODUCTION AND SIGNATURES OF DECONFINEMENT

J. RAFELSKI

Department of Physics, University of Arizona, Tucson, AZ 85721, USA

J. LETESSIER and A. TOUNSI

*Laboratoire de Physique Théorique et Hautes Energies
Université Paris 7, Tour 24, 2 Pl. Jussieu, F-75251 Cedex 05, France*

Using renormalization group methods we evaluate the thermal strangeness and charm chemical equilibrium relaxation times in the deconfined quark-gluon plasma. We present a reaction model and evaluate the total production rate of strangeness in fixed target Pb–Pb collisions at 10–300 A GeV. We discuss the relevance of our results to the diagnosis and understanding of the properties of the deconfined state.

1 Introduction

In high energy nuclear collisions¹ we are interested to create and study the deconfined quark-gluon phase, believed to consist in the limit of very high energy densities of a liquid of quarks and gluons interacting perturbatively. We are motivated by the desire to recreate in the laboratory conditions akin to those prevailing in the first moments of the Early Universe, and in the recognition that we can study the properties of the excited, ‘melted’, vacuum state of strong interactions.

Since in the collision of large nuclei the highly dense state is formed for a rather short time², one of the major challenges has been to identify suitable physical observables of deconfinement. A number of possible experimental signatures of the formation and properties of quark-gluon plasma (QGP) have been studied. This report addresses our recent advances in evaluating the relevance of strange^{3,4} and charm quark flavor in this quest⁴. Other major probes include the phenomenon of J/Ψ suppression⁵, photons and dileptons^{6,7}.

Strangeness is a very interesting diagnostic tool of dense hadronic matter⁸:

1) particles containing strangeness are found more abundantly in relativistic nuclear collisions than it could be expected based on simple scaling of p - p reactions;

2) all strange hadrons have to be made in inelastic reactions, while light u , d quarks are also brought into the reaction by the colliding nuclei;

3) because there are many different strange

particles, we have a very rich field of observables with which it is possible to explore diverse properties of the source;

4) theoretical calculations suggest that glue-gluon collisions in the QGP provide a sufficiently fast and thus by far a unique mechanism leading to an explanation of strangeness enhancement.

We begin by recalling these mechanisms of strangeness production. We then obtain in section 3 the magnitude of running coupling constant and quark masses. Using these results we evaluate the thermal relaxation times of strangeness and charm as function of temperature in section 4. We discuss the relevance of the flavor observable of QGP and describe how these relaxation times allow to compute the hadronic particle yields in section 5. We close with a few general remarks about the relevance of our results.

2 Strangeness Production in QGP

We will now show how to evaluate using two particle collision processes flavor production^{9,10} in thermal QGP. Ultimately, we will employ running QCD parameters $\alpha_s(\mu)$ and $m_i(\mu)$, $i = s, c$. While theory and experiment constrain now sufficiently the coupling strength α_s , considerable uncertainty still remains in particular in regard of strange quark mass scale, as well as systematic uncertainty related to applications of QCD to soft (less than 1 GeV) processes.

The generic angle averaged two particle cross

section for (heavy) flavor production processes $g + g \rightarrow f + \bar{f}$ and $q + \bar{q} \rightarrow f + \bar{f}$, are:

$$\bar{\sigma}_{gg \rightarrow f\bar{f}}(s) = \frac{2\pi\alpha_s^2}{3s} \left[\left(1 + \frac{4m_f^2}{s} + \frac{m_f^4}{s^2} \right) \cdot \tanh^{-1} W(s) - \left(\frac{7}{8} + \frac{31m_f^2}{8s} \right) W(s) \right], \quad (1)$$

$$\bar{\sigma}_{q\bar{q} \rightarrow f\bar{f}}(s) = \frac{8\pi\alpha_s^2}{27s} \left(1 + \frac{2m_f^2}{s} \right) W(s), \quad (2)$$

where $W(s) = \sqrt{1 - 4m_f^2/s}$, and both the QCD coupling constant α_s and flavor quark mass m_f will be in this work the running QCD parameters. In this way a large number of even- α_s diagrams contributing to flavor production is accounted for.

What remains unaccounted for is another class of processes in which at least one additional gluon is present. In particular processes allowing the production of an additional soft gluon in the final state remains unaccounted for today. Leading diagrams contain odd powers of α_s and their generic cross section is in general infrared divergent, requiring a cut-off which for processes occurring in matter is provided by the interactions (dressing) with other particles present. The process in which a massive ‘gluon’, that is a quasi-particle with quantum numbers of a gluon, decays into a strange quark pair, is partially included in the resummation that we accomplish in the present work. At the present time we do not see a systematic way to incorporate any residue of this and other effects, originating in matter surrounding the microscopic processes, as work leading to understanding of renormalization group equations in matter (that is at finite temperature and/or chemical potential) is still in progress¹¹.

3 Running QCD Parameters

To determine the two QCD parameters required, we will use the renormalization group functions β and γ_m :

$$\mu \frac{\partial \alpha_s}{\partial \mu} = \beta(\alpha_s(\mu)), \quad \mu \frac{\partial m}{\partial \mu} = -m \gamma_m(\alpha_s(\mu)). \quad (3)$$

For our present study we will use the perturbative power expansion in α_s :

$$\beta^{\text{pert}} = \alpha_s^2 \left[b_0 + b_1 \alpha_s + b_2 \alpha_s^2 + \dots \right], \quad \gamma_m^{\text{pert}} = \alpha_s \left[c_0 + c_1 \alpha_s + c_2 \alpha_s^2 + \dots \right], \quad (4)$$

For the SU(3)-gauge theory with n_f fermions the first two terms (two ‘loop’ order) are renormalization scheme independent, and we include in our calculations the three ‘loop’ term as well, which is renormalization scheme dependent, evaluated in the MS-scheme¹². We have:

$$b_0 = \frac{1}{2\pi} \left(11 - \frac{2}{3} n_f \right), \quad b_1 = \frac{1}{4\pi^2} \left(51 - \frac{19}{3} n_f \right), \quad (5)$$

$$b_2 = \frac{1}{64\pi^3} \left(2857 - \frac{5033}{9} n_f + \frac{325}{27} n_f^2 \right),$$

$$c_0 = \frac{2}{\pi}, \quad c_1 = \frac{1}{12\pi^2} \left(101 - \frac{10}{3} n_f \right), \quad (6)$$

$$c_2 = \frac{1}{32\pi^3} \left(1249 - \left(\frac{2216}{27} + \frac{160}{3} \zeta(3) \right) n_f - \frac{140}{81} n_f^2 \right).$$

The number n_f of fermions that can be excited, depends on the energy scale μ . We have implemented this using the exact phase space form appropriate for the terms linear in n_f :

$$n_f(\mu) = 2 + \sum_{i=s,c,b,t} \sqrt{1 - \frac{4m_i^2}{\mu^2}} \cdot \left(1 + \frac{2m_i^2}{\mu} \right) \Theta(\mu - 2m_i), \quad (7)$$

with $m_s = 0.16$ GeV, $m_c = 1.5$ GeV, $m_b = 4.8$ GeV. We checked that there is very minimal impact of the running of the masses in Eq. (7) on the final result, and will therefore not introduce that ‘feed-back’ effect into our current discussion. The largest effect on our solutions comes from the bottom mass, since any error made at about 5 GeV is amplified most. However, we find that this results in a scarcely visible change even when the mass is changed by 10% and thus one can conclude that the exact values of the masses and the nature of flavor threshold is at present of minor importance in our study.

We show the result of numerical integration for α_s in the top portion of Fig. 1. First equation in (3) is numerically integrated beginning with an initial value of $\alpha_s(M_Z)$. We use in this report the August 1996 World average¹³: $\alpha_s(M_Z) = 0.118$ for which the estimated error is ± 0.003 . This value is sufficiently precise to eliminate most of the uncertainty that has befallen much of our earlier studies^{4,10}. In addition, the thin solid lines present results for $\alpha_s(M_Z) = 0.115$ till recently the preferred result in some analysis, especially those at

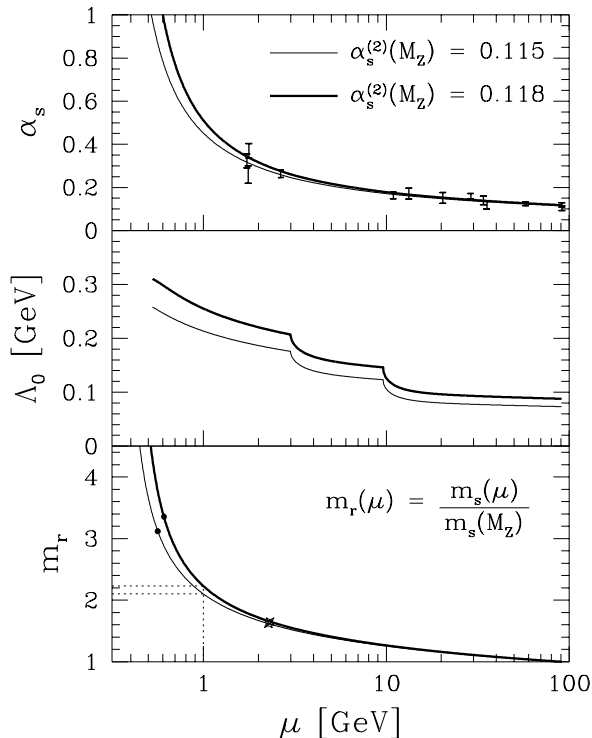


Figure 1: $\alpha_s(\mu)$ (top section); the equivalent parameter Λ_0 (middle section) and $m_r(\mu) = m(\mu)/m(M_Z)$ (bottom section) as function of energy scale μ . Initial value $\alpha_s(M_Z) = 0.118$ (thick solid lines) and $\alpha_s(M_Z) = 0.115$ (thin solid lines). In lower section the dots indicate the strangeness pair production thresholds for $m_s(M_Z) = 90$ MeV, while crosses indicate charm pair production thresholds for $m_c(M_Z) = 700$ MeV.

lower energy scale. As seen in Fig. 1, the variation of α_s with the energy scale is substantial, and in particular we note the rapid change at and below $\mu = 1$ GeV, where the strange quark flavor formation occurs in hot QGP phase formed in present day experiments at 160–200 A GeV (SPS-CERN). Clearly, use of constant value of α_s is hardly justified, and the first order approximation often used:

$$\alpha_s(\mu) \equiv \frac{2b_0^{-1}(n_f)}{\ln(\mu/\Lambda_0(\mu))^2}, \quad (8)$$

leads to a strongly scale dependent $\Lambda_0(\mu)$ shown in the middle section of Fig. 1. Thus it also cannot be used in the evaluation of thermal strangeness and charm production.

With $\alpha_s(\mu)$ from the solutions described above, we integrate the running of the quark masses, the second equation in (3). Because the

running mass equation is linear in m , it is possible to determine the universal quark mass scale factor

$$m_r = m(\mu)/m(\mu_0). \quad (9)$$

Since α_s refers to the scale of $\mu_0 = M_Z$, it is a convenient reference point also for quark masses. As seen in the bottom portion of Fig. 1, the change in the quark mass factor is highly relevant, since it is driven by the rapidly changing α_s near to $\mu \simeq 1$ GeV. For each of the different functional dependences $\alpha_s(\mu)$ we obtain a different function m_r . The significance of the running of the charmed quark mass cannot be stressed enough, especially for thermal charm production occurring in foreseeable future experiments well below threshold, which amplifies the importance of exact value of m_c .

Given these results, we find that for $\alpha_s = 0.118$ and $m_s(M_Z) = 90 \pm 18$ MeV a low energy strange quark mass $m_s(1 \text{ GeV}) \simeq 200 \pm 40$ MeV, in the middle of the standard range $100 < m_s(1 \text{ GeV}) < 300$ MeV. Similarly we consider $m_c(M_Z) = 700 \pm 50$ MeV, for which value we find the low energy mass $m_c(1 \text{ GeV}) \simeq 1550 \pm 110$ MeV, at the upper (conservative for particle production yield) end of the standard range $1 < m_c(1 \text{ GeV}) < 1.6$ MeV. There is another (nonperturbative) effect of mass running, related to the mass at threshold for pair production m_i^{th} , $i = s, c$, arising from the solution of:

$$m_i^{\text{th}}/m_i(M_Z) = m_r(2m_i^{\text{th}}). \quad (10)$$

This effect stabilizes strangeness production cross section in the infrared: below $\sqrt{s} = 1$ GeV the strange quark mass increases rapidly and the threshold mass is considerably greater than $m_s(1 \text{ GeV})$. We obtain the threshold values $2m_s^{\text{th}} = 611$ MeV for $\alpha_s(M_Z) = 0.118$ and $2m_s^{\text{th}} = 566$ MeV for $\alpha_s(M_Z) = 0.115$. Both values are indicated by the black dots in Fig. 1. For charm, the running mass effect plays differently: since the mass of charmed quarks is listed in tables for $\mu = 1$ GeV, but the value of the mass is above 1 GeV, the production threshold mass is smaller than expected (i.e., listed value). For $m_c(M_Z) = 700$ MeV the production threshold is found at $\sim 2m_c^{\text{th}} \simeq 2.3$ GeV rather than 3.1 GeV that would have been expected for the $m_c(1 \text{ GeV})$. This reduction in threshold enhances thermal production of charm, especially so at low temperatures.

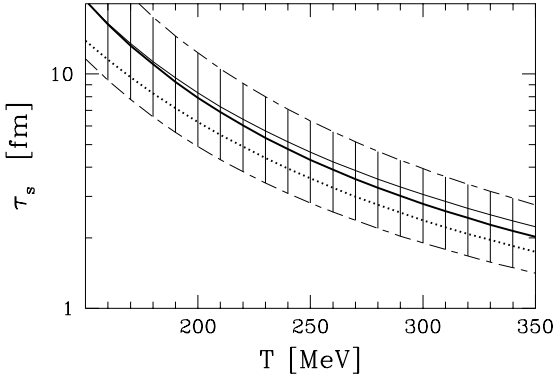


Figure 2: QGP strangeness relaxation time, for $\alpha_s(M_Z) = 0.118$, (thick line) and $= 0.115$ (thin line); $m_s(M_Z) = 90$ MeV. Hatched areas: effect of variation of strange quark mass by 20%. Dotted: comparison results for fixed $\alpha_s = 0.5$ and $m_s = 200$ MeV.

4 Strangeness and Charm Thermal Relaxation Times

The thermal average of the cross section is the invariant production rate per unit time and volume:

$$\begin{aligned}
 A_s &\equiv A_{gg} + A_{u\bar{u}} + A_{d\bar{d}} + \dots \\
 &= \int_{4m_s^2}^{\infty} ds 2s \delta(s - (p_1 + p_2)^2) \int \frac{d^3 p_1}{2(2\pi)^3 E_1} \\
 &\quad \times \int \frac{d^3 p_2}{2(2\pi)^3 E_2} \left[\frac{1}{2} g_g^2 f_g(p_1) f_g(p_2) \overline{\sigma_{gg}}(s) \right. \\
 &\quad \left. + n_f g_q^2 f_q(p_1) f_{\bar{q}}(p_2) \overline{\sigma_{q\bar{q}}}(s) + \dots \right]. \quad (11)
 \end{aligned}$$

The dots indicate that other mechanisms may contribute to strangeness production. The particle distributions f_i are in our case thermal Bose/Fermi functions (for fermions with $\lambda_q = 1.5$), and $g_q = 6$, $g_g = 16$. For strangeness production $n_f = 2$, and for charm production $n_f = 3$. From the invariant rate we obtain the strangeness relaxation time τ_s shown in Fig. 2, as function of temperature:

$$\tau_s \equiv \frac{1}{2} \frac{\rho_s^\infty(\tilde{m}_s)}{(A_{gg} + A_{qq} + \dots)}. \quad (12)$$

Note that here unaccounted for processes, such as the above mentioned odd-order in α_s would add to the production rate incoherently, since they can be distinguished by the presence of incoming/outgoing gluons. Thus the current calculation offers an upper limit on the actual relaxation time,

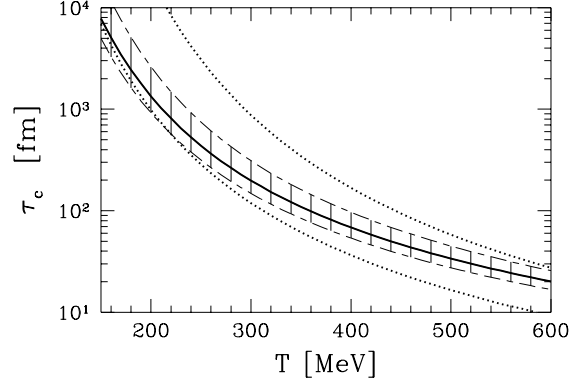


Figure 3: Solid lines: thermal charm relaxation constant in QGP, calculated for running $\alpha_s(M_Z) = 0.115; 0.118$, (indistinguishable), $m_c(M_Z) = 700$ MeV. Lower dotted line: for fixed $m_c = 1.1$ GeV, $\alpha_s = 0.35$; upper dotted line: for fixed $m_c = 1.5$ GeV, $\alpha_s = 0.4$. Hatched area: effect of variation $m_c(M_Z) = 700 \pm 50$ MeV

which may still be smaller. In any case, the present result suffices to confirm that strangeness will be very near to chemical equilibrium in QGP formed in collisions of large nuclei.

We show in Fig. 2 also the impact of a 20% uncertainty in $m_s(M_Z)$, indicated by the hatched areas. This uncertainty is today much larger compared to the uncertainty that arises from the recently improved precision of the strong coupling constant determination¹³. We note that the calculations made⁹ at fixed values $\alpha_s = 0.5$ and $m_s = 200$ MeV (dotted line in Fig. 2) are well within the band of values related to the uncertainty in the strange quark mass.

Since charm is somewhat more massive compared to strangeness, there is still less uncertainty arising in the extrapolation of the coupling constant. Also the systematic uncertainty related to the soft gluons (odd- α_s) terms are smaller, and thus the relaxation times τ_c we show in Fig. 3 are considerably better defined compared to τ_s . There is also less relative uncertainty in the value of charm mass. We also show in Fig. 3 (dotted lines) the fixed m_c, α_s results with parameters selected to border high and low T limits of the results presented. It is difficult to find a good comparative behavior of τ_c using just one set of m_c and α_s . This may be attributed to the importance of the mass of the charmed quarks, considering that the threshold for charm production is well above the average thermal collision energy, which results

in emphasis of the effect of running charm mass. In the high T -limit the choice (upper dotted line in Fig. 3) $m_c = 1.5$ GeV, $\alpha_s = 0.4$ is appropriate, while to follow the result at small T (lower dotted line in Fig. 2) we take a much smaller mass $m_c = 1.1$ GeV, $\alpha_s = 0.35$.

We recall that the equilibrium distribution is result of Boltzmann equation description of two body collisions. Thus the mass arising in the equilibrium density ρ_s^∞ in Eq. (12) is to be taken at the energy scale of the average two parton collision. We adopt for this purpose a fixed value $\tilde{m}_s = 200$ MeV, and observe that in the range of temperatures here considered the precise value of the mass is insignificant, since the quark density is primarily governed by the T^3 term in this limit, with finite mass correction being $\mathcal{O}(10\%)$. The situation is less clear for charm relaxation, since the running of the mass should have a significant impact. Short of more complete kinetic treatment, we used $m_c \simeq 1.5$ GeV in order to establish the reference density ρ_c^∞ in Eq. (12).

5 QGP Flavor Observable

We will indicate in this section how the study of flavor production impacts our understanding and diagnosis of the deconfined QGP phase. We recall first that there are two generic flavor observable which we can study analyzing experimental data:

- **yield of strangeness/charm:**

once produced in hot early QGP phase, strangeness/charm is not reannihilated in the evolution of the deconfined state towards freeze-out, and thus the flavor yield is characteristic of the initial, most extreme conditions;

- **phase space occupancy $\gamma_{s,c}$:**

impacts distribution of flavor among final state particle abundances.

Given that the thermal equilibrium is established within a considerably shorter time scale than the (absolute) heavy flavor chemical equilibration, we can characterize the equilibration of the phase space occupancy by an average over the momentum distribution:

$$\gamma_i(t) \equiv \frac{\int d^3p d^3x n_i(\vec{p}, \vec{x}; t)}{\int d^3p d^3x n_i^\infty(\vec{p}, \vec{x})}, \quad i = s, c. \quad (13)$$

The chemical equilibrium density is indicated by upper-script ‘ ∞ ’. When several carriers of the

flavor are present, as is the case in the confined phase, n_i is understood to comprise a weighted sum.

In order to be able to compute the production and evolution of strangeness and charm flavor a more specific picture of the temporal evolution of dense matter is needed. Here, we will address specifically strangeness production in collisions at CERN-SPS, up to 200 A GeV per nucleon. We use a simple, qualitative description, simplified by the assumption that the properties of the hot, dense matter are constant across the entire volume (fireball model). We consider radial expansion to be the dominant factor for the evolution of the fireball properties such as temperature/energy density and lifetime of the QGP phase. Within the fireball model the expansion dynamics follows from two assumptions:

- the (radial) expansion is entropy conserving, thus the volume and temperature satisfy:

$$V \cdot T^3 = \text{Const.} \quad (14)$$

- the surface flow velocity is given by the sound velocity in a relativistic gas

$$v_f = 1/\sqrt{3}. \quad (15)$$

This leads to the explicit forms for the radius of the fireball and its average temperature:

$$R = R_{\text{in}} + \frac{1}{\sqrt{3}}(t - t_{\text{in}}), \quad T = \frac{T_{\text{in}}}{1 + (t - t_{\text{in}})/\sqrt{3}R_{\text{in}}}.$$

The initial conditions for Pb–Pb:

$\lambda_q = 1.6$, $t_{\text{in}} = 1$ fm/c, $T_{\text{in}} = 320$ MeV; with $R_{\text{in}} = 4.5$ fm for $\eta = 0.5$; $R_{\text{in}} = 5.2$ fm for $\eta = 0.75$, and for S–Pb/W:

$\lambda_q = 1.5$, $t_{\text{in}} = 1$ fm/c, $T_{\text{in}} = 280$ MeV; with $R_{\text{in}} = 3.3$ fm for $\eta = 0.35$; $R_{\text{in}} = 3.7$ fm for $\eta = 0.5$, have been determined such that the energy per baryon is given by energy and baryon flow, and the total baryon number is $\eta(A_1 + A_2)$, as stopped in the interaction region. The radius shown above are for zero impact parameter. For this, equations of state of the QGP are needed, and we have employed our model¹⁴ in which the perturbative correction to the number of degrees of freedom were incorporated along with thermal particle masses.

In the fireball in every volume element we have:

$$n_s(\vec{p}; t) = \gamma_s n_s^\infty(\vec{p}; T, \mu_s). \quad (16)$$

Table 1: γ_s and N_s/B in S–W at 200 A GeV and Pb–Pb at 158 A GeV for different stopping values of baryonic number and energy $\eta_B = \eta_E$; computed for strange quark mass $m_s(1\text{GeV}) = 200 \pm 40$ MeV, $\alpha_s(M_Z) = 0.118$.

E_{lab}	S–W at 200 A GeV		Pb–Pb at 158 A GeV	
$\eta_B = \eta_E$	0.35	0.5	0.5	0.75
γ_s	0.53 ± 0.14	0.65 ± 0.15	0.69 ± 0.15	0.76 ± 0.16
N_s/B	0.67 ± 0.16	0.70 ± 0.16	0.954 ± 0.20	0.950 ± 0.20

In this limit and allowing for the detailed balance reactions, thus re-annihilation of flavor, the yield is obtained from the equation:

$$\frac{dN_s(t)}{dt} = V(t)A_s [1 - \gamma_s^2(t)]. \quad (17)$$

Allowing for dilution of the phase space density in expansion, we derive⁴ from Eq. (17) an equations describing the change in $\gamma_s(t)$:

$$\frac{d\gamma_s}{dt} = \left(\gamma_s \frac{\dot{T}m_s}{T^2} \frac{d}{dx} \ln x^2 K_2(x) + \frac{1}{2\tau_s} [1 - \gamma_s^2] \right). \quad (18)$$

Here K_2 is a Bessel function and $x = m_s/T$. Note that even when $1 - \gamma_s^2 < 1$ we still can have a positive derivative of γ_s , since the first term on the right hand side of Eq. (18) is always positive, both \dot{T} and $d/dx(x^2 k_2)$ being always negative. This shows that dilution due to expansion effects in principle can make the value of γ_s rise above unity.

Given the relaxation constant $\tau_s(T(t))$, these equations can be integrated numerically, and we can obtain for the two currently explored experimental systems the values of the two observables, γ_s and N_s/B , which are given in table 1.

For S–Ag collisions at 200 A GeV a recent evaluation of the specific strangeness yield leads to $N_s/B|_{\text{exp}} = 0.86 \pm 0.14$ (see table 4 of Ref.¹⁵). Our earlier analysis⁴ of the WA85 data yields $\gamma_s = 0.75 \pm 0.1$ for S–W interactions. Both these results are in good agreement with the theoretical result shown in the table, favoring the 50% stopping case for S–W. The analysis of the experimental Pb–Pb data is in progress.

As we can see in table 1, there is a considerable uncertainty due to the unknown mass of strange quarks. On the other hand, inspecting the yield of strange quarks per baryon N_s/B there

seem to be very little dependence on the stopping fractions. This insensitivity to the reaction mechanism coupled to a visible sensitivity to strange quark mass suggests that additional insight may be ultimately gained about the strange quark mass from the study of strangeness enhancement in relativistic heavy ion collisions. Thus we show in Fig. 4 as function of $m_s(M_Z)$ for the two different stopping fractions the resulting strangeness yield per baryon, N_s/B . The range of strange quark mass shown corresponds to the allowed range $45 < m_s(M_Z) < 135$ MeV ($100 \lesssim m_s(1\text{ GeV}) \lesssim 300$ MeV). The known systematic and statistical error is indicated by the divergence of the different curves, and is particularly small for N_s/B .

Before we can use these results to obtain a more reliable estimate of strange quark mass, we will need to understand other sources of systematic uncertainty, e.g., those associated with unknown mechanisms of strangeness production and

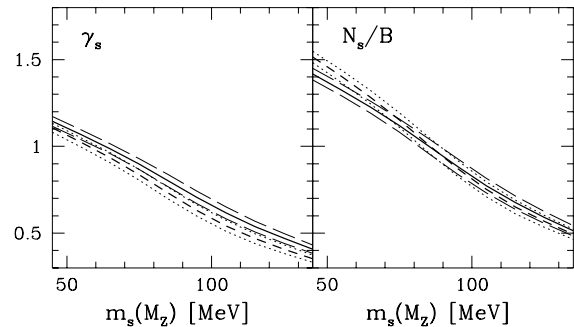


Figure 4: Phase space occupancy γ_s and yield of strange quarks per baryon N_s/B as function of strange quark mass $m_s(M_Z)$ for Pb–Pb collision system at 158 A GeV, for the two stopping fractions and $\alpha_s(M_Z) = 0.118 \pm 0.003$: thick solid lines, $\eta = 75\%$, with long dashed lines indicating the $\alpha_s(M_Z)$ uncertainty, thick dashed lines for $\eta = 50\%$, with dotted lines indicating the $\alpha_s(M_Z)$ uncertainty.

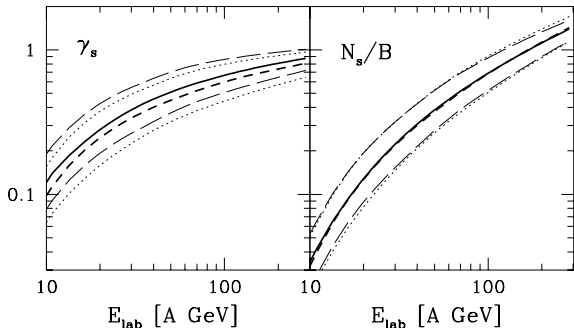


Figure 5: Phase space occupancy γ_s and yield of strange quarks per baryon N_s/B as function of laboratory collision energy in Pb–Pb interactions for $m_s = 200 \pm 40$ MeV and two different stopping fractions: $\eta = 50\%$ (dashed and two dotted lines) and $\eta = 75\%$ (solid and two long dashed lines).

to improve the model of QGP we are employing. However, these results are so strongly dependent on m_s and so little on other quantities, that we can be optimistic that one day strange and charm flavor mass may be obtained from the flavor yields seen in nuclear collisions.

Assuming that the model we proposed has been effectively tested at 200 A GeV S–W/Pb collisions, we compute the strangeness yield and phase space occupancy as function of energy. The results are shown for the case of Pb–Pb collisions. We show these results in Fig. 5 as function of laboratory collision energy, stressing that if at low energies the QGP phase is not encountered, we would expect to see a drop in strangeness yield beyond the expectations here presented.

These results allow us to evaluate the strange (anti)baryon yields from QGP as function of collision energy. We note that at fixed m_\perp the medium dependent factor controlling the abundance of hadrons emerging from the surface of the deconfined region is related to the chemical conditions in the source, and for strange quarks, there is also the occupancy factor γ_s to be considered:

$$n_h|_{m_\perp} = e^{-m_\perp/T} \prod_{k \in h} \gamma_k \lambda_k. \quad (19)$$

The strange quark fugacity is in deconfined phase unity, while the light quark fugacity evolution with energy of colliding ions follows from our earlier studies¹⁴. In Fig. 6. we have normalized all yields at $E_{\text{Lab}} = 158$ A GeV. Remarkably, all antibaryon yields (left hand side of Fig. 6) cluster

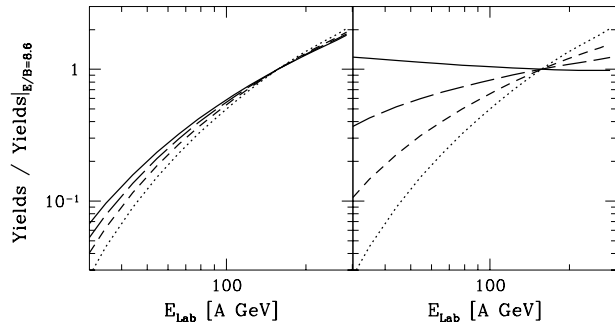


Figure 6: Relative yields of antibaryons (left) and baryons (right) as function of heavy ion collision energy E_{Lab} . Abundance set to a common value (unity) at $E_{\text{Lab}} = 158$ A GeV. Solid lines: nucleons, long dashed $\Lambda + \Sigma^0$, short dashed Ξ , dotted Ω .

together (solid lines: (anti)nucleons, long dashed: (anti)hyperons, short-dashed: (anti)cascades, and dotted: (anti)omegas), thus as long as the QGP phase is formed, ratios of rare multi-strange antibaryons should not change significantly while the collision energy is reduced, until the QGP formation is disrupted. It should be noted that the yield of $\bar{\Omega}$ remains appreciable, all the way even at very small energies — this is the case as long as these particles are produced by the deconfined phase, rather than in individual hadronic interactions. For baryons (right hand side of Fig. 6) there is considerable differentiation of the yield behavior: the reference yield of nucleons rises slightly to compensate for the drop in the yield of other strange baryons, which decreases substantially with energy.

6 Final Remarks

In conclusion, we can once more remind ourselves about the two generic strangeness observables. The relative total abundance of strangeness is most related to the initial condition, the ‘hotter’ the initial state is, the greater the production rate, and thus the final state relative yield, to be measured with respect to baryon number or global particle multiplicity (entropy). The phase space occupancy of strangeness γ_s depends aside of the initial production rate, on the final state dilution characterized by dynamics of the expansion and the freeze-out temperature. Our results show that we can use certain features of strange particle production to see the formation of the deconfined state and to study some QCD properties

and parameters. Our results suggest that already at present energies deconfinement is attained, and we have explored a number of features as function of collision energy in order to see if a more systematic study is capable to confirm this conclusion.

Using QCD renormalization group methods we have studied the s and c flavor chemical equilibrium relaxation times. We have shown that the newly measured QCD coupling constant comprises sufficiently small uncertainty to allow precise evaluation of strangeness production at and below 1 GeV energy scale. Our study has further proven that it is essential to incorporate in the evaluation of flavor production rates both running coupling constant *and* running mass.

We find that running of the QCD parameters is of major significance, since, e.g., the effective charm production mass is considerably reduced, seen on the scale of available thermal energies. We found considerable enhancement of charm production for temperatures applicable at SPS collision energy, compared to fixed mass results. While charm experiences at low temperature $T \simeq 200$ MeV a 100 times slower approach to chemical equilibrium compared to strangeness, for temperatures of about 500 MeV, as may apply to the conditions generated at LHC or perhaps even RHIC collider, $\tau_c \rightarrow 30$ fm, which is within factor two of the expected maximum lifespan of the deconfined state. Thus our calculations suggest that there will be a significant abundance of thermal charm in nuclear interactions at RHIC/LHC. In consequence, open charm should play a similar role in the diagnosis of the ‘hot’ $T \simeq 500$ MeV deconfined state as strangeness is playing today for the ‘cold’ $T \simeq 250$ MeV case, and charm equilibrium appears within reach of the extreme conditions possibly arising at LHC.

Our here presented results imply that in key features the strange particle production results obtained at 160–200 A GeV, are consistent with the QGP formation hypothesis. However, in order to ascertain the possibility that indeed the QGP phase is already formed today, a more systematic experimental exploration as function of collision energy of the different observable is required, for which purpose we also have explored the collision energy dependence of the most characteristic strange particle features expected from the QGP phase.

Acknowledgments

J.R. acknowledges partial support by DOE, grant DE-FG03-95ER40937.
LPTHE: Unité associée au CNRS UA 280.

References

1. R. Stock, *High Energy Nuclear Interactions and Heavy Ion Collisions*, in this proceedings.
2. J.D. Bjorken, *Phys. Rev.* **D27**, 140 (1983).
3. G. Odyniec, *Intriguing Results on Strangeness Production at CERN-SPS Energies*, in this proceedings.
4. J. Rafelski, J. Letessier and A. Tounsi, *Acta Phys. Pol.* **B27**, 1035 (1996); and references therein.
5. P. Petiau, *Anomalous J/Ψ Suppression in Pb–Pb Interactions at 158 A GeV/c*, in this proceedings.
6. A. Pfeiffer, *Low-mass Electron Pair Production in Pb–Au Collisions at the CERN SPS — New Results from the CERES/NA45 Experiment*, in this proceedings.
7. K. Redlich, *Soft Dilepton Production in Ultrarelativistic Heavy Ion Collisions at SPS Energy*, in this proceedings.
8. J. Rafelski, Ed., *Strangeness in Hadronic Matter*, American Institute of Physics Conference Proceedings 340, New York 1995.
9. T. Biró and J. Zimányi, *Phys. Lett.* **B113** (1982) 6; *Nucl. Phys.* **A395** (1983) 525; J. Rafelski and B. Müller, *Phys. Rev. Lett.* **48** (1982) 1066; **56** (1986) 2334E.
10. J. Letessier, J. Rafelski, and A. Tounsi, *Impact of QCD and QGP properties on strangeness production*, *Phys. Lett. B. in press* (1996).
11. P. Elmfors and R. Kobes, *Phys. Rev.* **D51**, 774 (1995).
12. L.R. Surguladze and M.A. Samuel, *Rev. Mod. Phys.* **68** (1996) 259.
13. M. Schmelling, *Status of the Strong Coupling Constant*, in this proceedings.
14. J. Letessier, J. Rafelski, and A. Tounsi, *Phys. Lett.* **B333**, 484 (1994); **B323**, 393 (1994).
15. M. Gaździcki and D. Röhrich, *Strangeness in Nuclear Collisions* preprint IKF-HENPG/8-95, *Z. Physik C* (1996).